# **RESEARCH PAPER**

# Preparation and Characterization of Nanofibers Composed of Fullerene, Gold Nanoparticles, PAni, and PVA for Medical Biosensor Fabrication Using the Electrospinning Method

AbdulRahman Hammad Jasim 1\*, Kamel Said 1, M. A. Alalousi 2

### ARTICLE INFO

#### Article History:

Received 02 September 2025 Accepted 10 November 2025 Published 01 January 2026

# Keywords:

Cyclic Voltammetry Elictrospinning Fullerene Laser ablation XRD

### **ABSTRACT**

The aim of this study is to prepare nanofibers from fullerenes and gold nanoparticles at concentration of (0, 0.4, 1.9 and 3.6) ppm with PAni and PVA, for medical biosensor fabrication using the electrospinning method and to study the effect of both gold nanoparticles and fullerenes on the structural, morphological, XRD and Cyclic Voltammetry properties of nanofibers. The gold nanoparticles are causing pressure in the crystal lattices of the carbon materials ( $C_{80}$ ,  $C_{70}$ , and  $C_{60}$  polymers), Also These systematic displacements are not due to mere physical mixing, but rather are conclusive evidence of a real interaction at the atomic/crystal scale between gold and carbon , nanofibers with sizes ranging from 21.99 nm to 80.5 nm appeared, as did small, the sensor based on AuNP/CNF/PAni/PVA on a gold electrode exhibits a clear dose – dependent electrochemical response, this medical biosensor capable of reliably detecting CA II in the 0-125 ng/ml range.

## How to cite this article

Hammad Jasim A., Said K., Alalousi M. A. Preparation and Characterization of Nanofibers Composed of Fullerene, Gold Nanoparticles, PAni, and PVA for Medical Biosensor Fabrication Using the Electrospinning Method. J Nanostruct, 2026; 16(1):279-287. DOI: 10.22052/JNS.2026.01.025

# INTRODUCTION

In recent years, biosensors have become a crucial focus in research related to medical diagnostics and environmental monitoring, due to their ability to deliver precise and sensitive results for detecting a wide range of biomolecules. However, significant challenges remain in improving the sensitivity and stability of these sensors. Medical biosensors, in particular, require continuous performance enhancement to ensure accuracy and reliability [1]. While nanomaterials such as gold and carbon can significantly enhance the sensitivity of biosensors, their high cost

and the intricacies of manufacturing remain substantial hurdles [2]. Gold nanoparticles exhibit unique properties, such as high electrical conductivity and a large surface area, which make them highly effective in improving the sensitivity for detecting biomolecules [3]. Carbon nanotubes, on the other hand, offer exceptional mechanical and electrical properties that enhance the stability and extend the operational lifespan of sensors [4]. Additionally, Poly Aniline (PAni), a conductive polymer, is known for its ability to interact with ions and biomolecules, enhancing the sensitivity of sensors while contributing to

<sup>&</sup>lt;sup>1</sup> Laboratory of Ceramics Composites and Polymers Materials, Faculty of Sciences of Sfax, University of Sfax, Tunisia

<sup>&</sup>lt;sup>2</sup> University of Anbar, Al Anbar, Iraq

<sup>\*</sup> Corresponding Author Email: abdajeely@gmail.com

improved stability [5]. Furthermore, Poly Vinyl Alcohol (PVA) is a biodegradable polymer that can be used as a support material in medical sensor fabrication, reducing costs while promoting environmental sustainability [6]. The integration of gold nanoparticles and carbon nanotubes with PAni and PVA offers several potential benefits for improving the performance of biosensors. This combination enhances both electrical conductivity and sensitivity, allowing for more accurate detection of biomolecules [7, 5]. The addition of carbon nanofibers to PAni contributes to long-term sensor stability, making these devices more reliable across various environments [8, 9]. Using PVA as a supporting material provides an economical solution, reducing manufacturing costs, as it is a biodegradable polymer that minimizes environmental waste [10, 11].

In terms of potential applications, these enhanced sensors could significantly improve the early detection of tumors, increasing the effectiveness of early-stage disease diagnosis [12]. The flexibility of PAni and PVA also makes them suitable for developing wearable medical devices, providing continuous monitoring of health parameters with greater comfort and safety [13, 14]. Additionally, PVA can be used to create implantable sensors that offer long-term disease monitoring while safely degrading within the body over time [15].

Nevertheless, several challenges must still be

addressed, such as improving the biocompatibility of the materials to ensure they the body. Achieving long-term stability in diverse biological and chemical environments also requires further refinement of material formulations [16,17]. Additionally, the manufacturing processes need to be optimized to be more cost-effective and scalable, while ensuring high-quality sensor performance [18].

### **MATERIALS AND METHODS**

In this study several instruments and materials Suppliers: Carbon electrodes from dray batteries, gold, Distilled Deionized Water (DDW), Alcohol, 96% Acetone. To prepare the colloidal solution of carbon according to a previous study [19] to produce nanoparticles of gold and fullerene, the carbon was placed in 4 beakers, each beaker containing 50 ml of deionized water, and each one was bombarded with 3000 laser shots, then the gold was also bombarded with a number of laser shots: (0, 1000, 2000, 3000) respectively, with a laser beam using an Nd -YAG pulsed laser, its Parameter Value: Wavelength 1064 nm, the diameter of the spot 2 mm, the laser energy was 100 mJ, the pulse duration 6 Hz and laser pulse width 10 nm. The distance between the surface of solution and the laser lens was 12 cm Fig. 1.

After preparing the 50 ml colloidal solution, put it in the syringe of the electrospinning device Fig. 2. The electrospinning device was used with specific

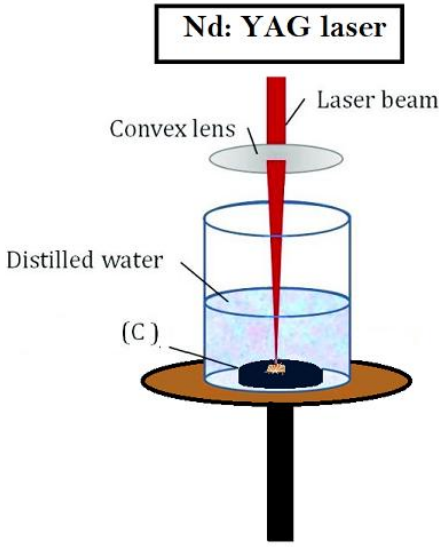


Fig. 1. Schematic illustration of the laser ablation method in liquid.

J Nanostruct 16(1): 279-287, Winter 2026



parameters. The distance between the needle and the sample in the rotating cylinder was 10 cm, the high voltage between them was 23.5 KV,

the cylinder rotated around its axis at a speed of 3000 rpm, and the colloidal fluid flow rate in the injection system was equal to 0.1 ml per hour, the colloidal solution exits from the nozzle of the syringe head, which is the positive pole, to the opposite rotating cylinder, that negative pole.

### **RESULTS AND DISCUSSION**

By analysis of X-ray diffraction (XRD)patterns (x-ray Anode Material Cu Generator Settings radiation and accelerated voltage of 40 kV and 30 mA). Williamson-Hall relation was [20] applied to estimate the crystalline size

$$D_{hkl} = \left(\frac{A\lambda}{\cos\theta. B_{hkl}}\right) + (4\epsilon\sin\theta) \tag{1}$$

FE-SEM images achieved via field emission scanning electron microscope (FE-SEM, INSPECT-550) have been used to evaluate the morphological properties of the prepared film surfaces, addition to the energy dispersive x-ray

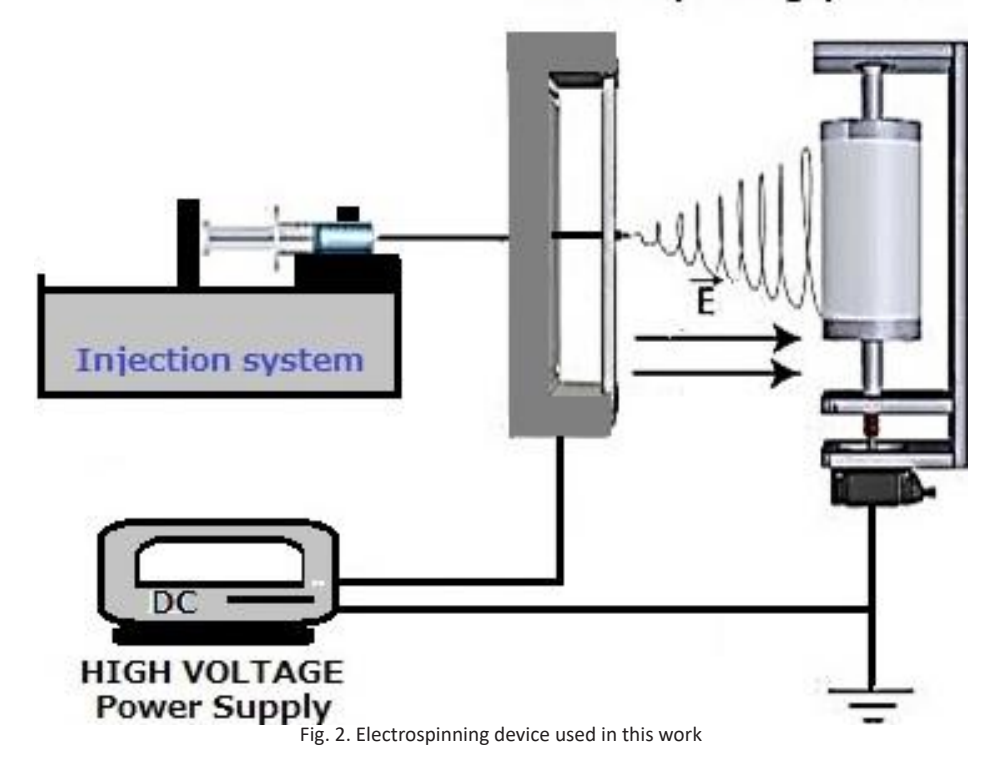
(EDX) microanalysis to estimate elemental analysis associated with the prepared films, as well Raman spectra were achieved to detect their vibrational and rotational.

XRD patterns have been analyzed based on COD 96-900-1992, ICSD 98-041-2242, ICDD 01-089-8491, ICSD 98-005-6668, and ICSD 98-009-6620 cards. Pure carbon films showed a polycrystalline structure with the dominance of  $C_{70}$  phases at 20 of approximately 20.33°, 22.83°, 29.04°, and 39.66°. The dominant phase was observed at about 29.04° (242) with crystallite size found at about 89.22 nm. Likewise, the presence of three main phases,  $C_{80}$ ,  $C_{70}$  and  $C_{60}$ - Polymer but with lower attributions as shown in Fig. 3.

Experimental location of the first reference curve (without gold)

In the first curve, the reference  $C_{80}$  peak is the peak at 13.5547°. We note that the second curve (0.4 ppm) at 15.9907° appears to be shifted significantly to the right (+2.436°). Curve 3 (1.9 ppm) at 16.0038° appears to be shifted significantly to the right (+2.449°). Curve 4 (3.6 ppm) at 15.8213° appears to be shifted significantly to the

# Electrospinning process



right (+2.266°). We conclude that the addition of gold caused a systematic and significant shift of the C<sub>80</sub> peaks toward higher (right) angles. C<sub>70</sub> peaks, which is the second indicator in the tables - the most important peak, the reference is the peak 20.3254°, where we notice curve 2 (0.4 ppm): 20.3161° shows a very slight shift to the left (-0.0093°). As for curve 3 (1.9 ppm): 20.5815°, there is also a clear shift, but to the right (+0.2561°). In curve 4 (3.6 ppm): 20.3503°, also a shift to the right (+0.0249°). We conclude that the behavior is more complex. At low concentration (0.4 ppm), the position is almost unchanged, but with increasing concentration, a shift to the right occurs, which is more pronounced at medium concentration (1.9 ppm). Polymer C<sub>60</sub> peaks, which is index 9 in the tables, the first reference curve is the peak 73.1248° and the second curve (0.4 ppm): 73.5587° appears to be shifted to the right by (+0.4339°), and in the third curve (1.9 ppm also the peak): 73.3975° shifted to the right by (+0.2727°), and the fourth curve (3.6 ppm): 73.4005° in the peak shifted to the right (+0.2757°).

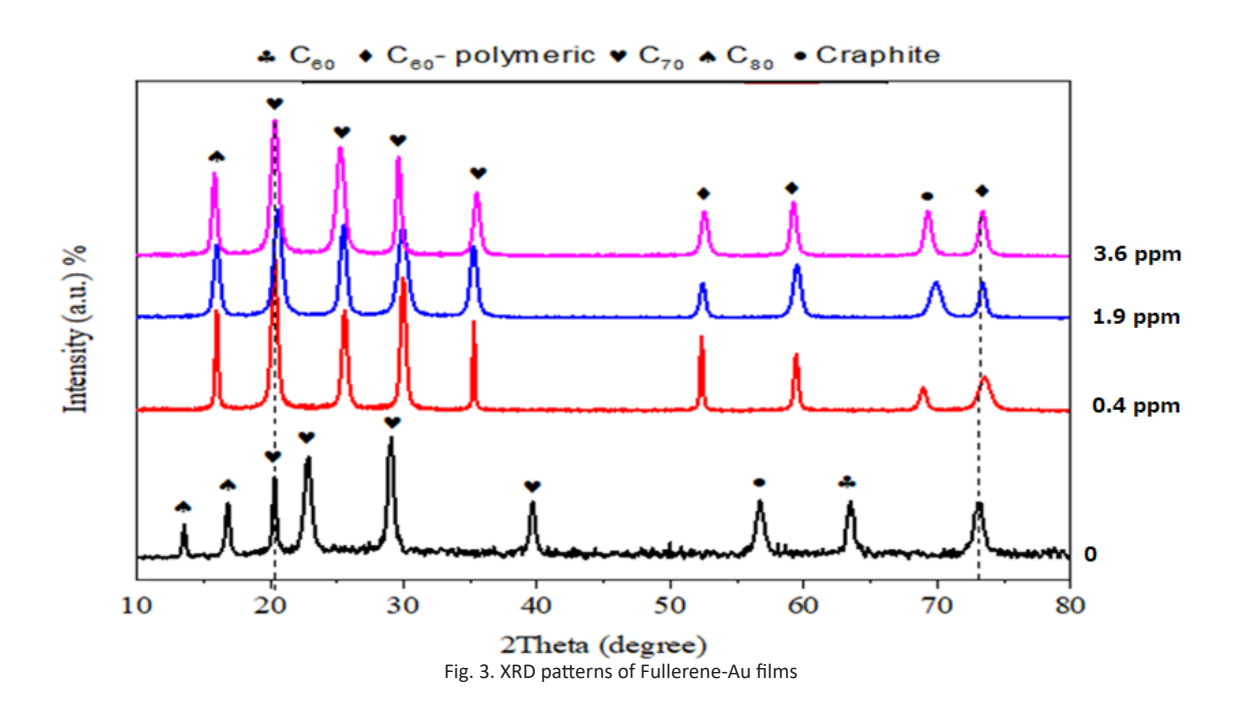
The shift in diffraction angle (20) is directly related to the change in the distance between crystal planes (d-spacing) according to Bragg's law:

nλ = 2d sinθ

Rightward shift (increasing  $\theta$ ): This means a decrease in the distance (d) between crystal planes. Physical Interpretation: This often indicates compressive strain within the crystal lattice. The introduction of smaller gold atoms or particles (or their formation in interstitial sites) can compress and bring the crystal planes closer together, leading to a decrease in the value of d and thus an increase in the angle  $\theta$ .

Leftward shift (decreasing  $\theta$ ): This means an increase in the distance (d) between crystal planes. This indicates a tensile strain within the lattice. This very slight displacement was observed in one case (C<sub>70</sub> at 0.4 ppm), and may be due to the presence of impurities or an initial surface interaction causing a slight expansion.

- 1. The dominant effect is pressure: The dominant and clear displacement direction in your data is to the right, which means that the gold nanoparticles are causing pressure in the crystal lattices of the carbon materials ( $C_{80}$ ,  $C_{70}$ , and  $C_{60}$  polymers). This pressure leads to a decrease in the distances between the atomic planes.
- 2. Evidence of interaction: These systematic displacements are not due to mere physical mixing, but rather are conclusive evidence of a real interaction at the atomic/crystal scale between



gold and carbon. The gold particles are not just sitting on the surface; they permeate the structure and create internal stress.

3. Concentration and structure dependence: The magnitude of the response (amount of displacement) varies depending on the type of carbon molecule ( $C_{80}$  was most affected) and the gold concentration, indicating that the reaction mechanism and the extent of each structure's influence may differ.

The rightward shift of the peaks is direct experimental evidence that nanogold exerts pressure on the carbon crystal structures, altering their fundamental physical properties. This is critical to the performance of the hybrid material in various applications such as catalysis and electronics.

Fig. 4 represents FE-SEM images that mainly give morphological information about the surface of the prepared Fullerenes and AuNPs-fullerene nanofiber with 0, 0.4, 1.9, and 3.6 ppm.

A clear separation was observed between the different particles, especially the nanofibers, which are believed to be C60 polymers with an average diameter of approximately 39 nm, as shown in Fig. 4. The addition of gold nanoparticles led to a clear change in the stages of nanofiber formation. The addition of gold at concentrations of 0, 0.4, 1.9, and 3.6 ppm resulted in a variety of formations,

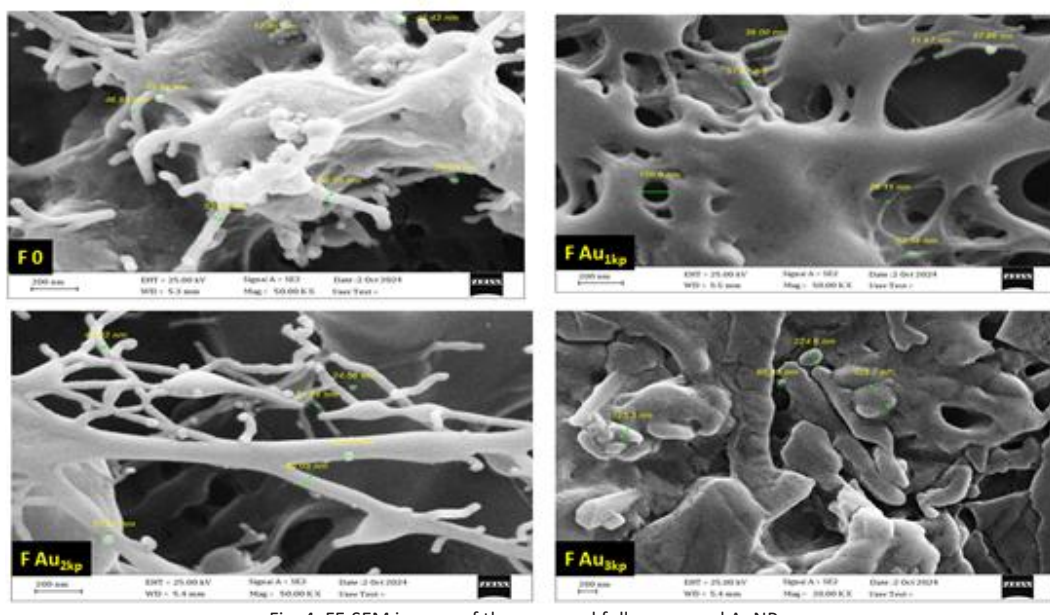
consisting of scattered spherical particles with diameters ranging from 17.86 to

35.73 nm in the absence of gold. In addition, hairs with a thickness of approximately 29 nm to 42 nm and nanofibers with a diameter of approximately 53 nm also appeared. At a concentration of 0.4 ppm, nanofibers with sizes ranging from 21.99 nm to 80.5 nm appeared, as did small, few-numbered spheres with diameters ranging from 24.56 nm to 42.43 nm, which are believed to be either gold or a by-product of the nanofibers due to the high speed of the collecting drum. At a concentration of 1.9 ppm, holes appeared in the tissue with diameters ranging from 37.9 nanometers to 120.6 nanometers. Increasing the concentration of gold nanoparticles to 3.6 ppm led to the appearance of large random clusters, while the spheres had diameters ranging from 224.6 nanometers to 422.7 nanometers, as shown in Fig. 4.

### Cyclic Voltammetry test

Here, the results of cyclic voltammetry (CV) analysis of nanofibers fabricated as biosensors are presented, using a mixture of carbon nanoparticles and gold nanoparticles at varying concentrations of carbon and carbon-gold (0, 0.4, 1.9 and 3.6) ppm.

The electrodes were fabricated by depositing gold on a square piece of glass with a mask, then



Last Attempt - Successfully Obtained Fiber and Good Measurements

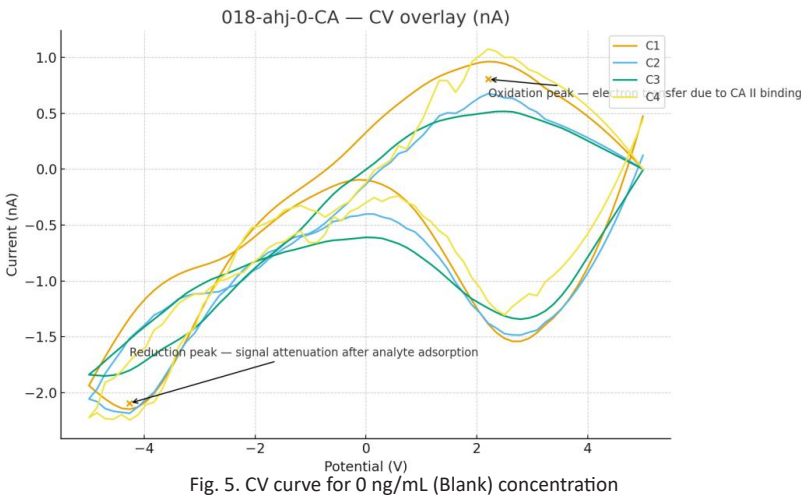
Fig. 4. FE-SEM images of the prepared fullerenes and AuNPs-

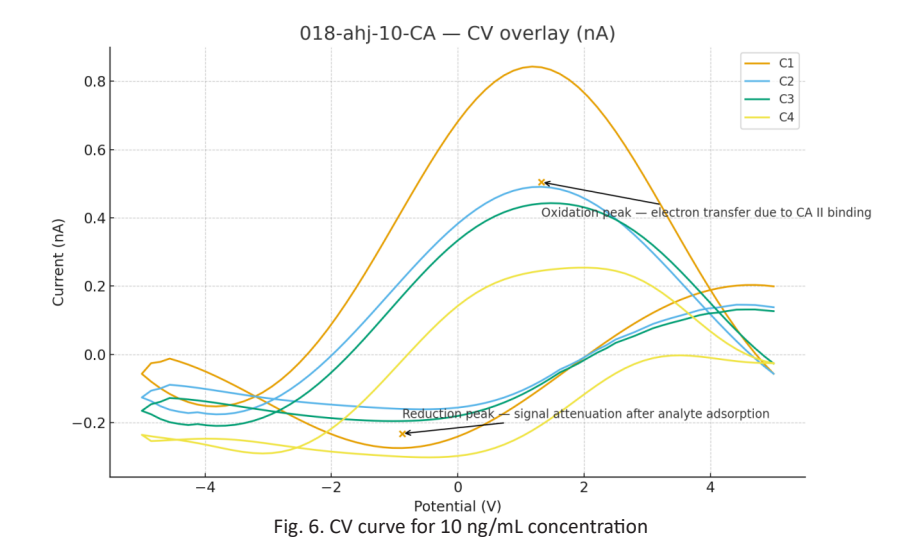
depositing the aforementioned mixture onto the nanofiber electrodes using an electrospray. The biosensor was supplied with a voltage ranging from -5 V to +5 V. The voltage between the electrodes and the current flowing through them were measured after applying different concentrations of CAII to each experiment over four cycles for subsequent study and evaluation of the sensor. The current intensity often increases with increasing CAII concentration. Redox signals are considered an indicator and diagnostic of fullerene interactions with tumor [21]. The inclusion of gold electrodes also improved the currents, due to the nature of gold nanoparticles, which provides a large surface area that enhances

the interaction, which is crucial for enhancing the sensitivity of chemical sensing. The large surface area of gold nanoparticles allows for greater adhesion of reagents, which promotes increased interaction between the analyte and the biological receptor, thus amplifying signal transmission. Gold nanoparticles (AuNPs) are considered an ideal support for the development of sensors, due to their properties, most notably good conductivity and high surface area [22, 23, 24].

# 0 ng/mL (Blank)

In the absence of CA II, the electrode surface remains fully active, resulting in a relatively high oxidation peak current (≈0.76 nA) and a





J Nanostruct 16(1): 279-287, Winter 2026

total charge of  $\approx$  –18.4 nC. This reflects efficient electron transfer through the AuNP/CNT/PAni/PVA film layer. This condition represents the baseline response, which is used for comparison with the other tested concentrations.

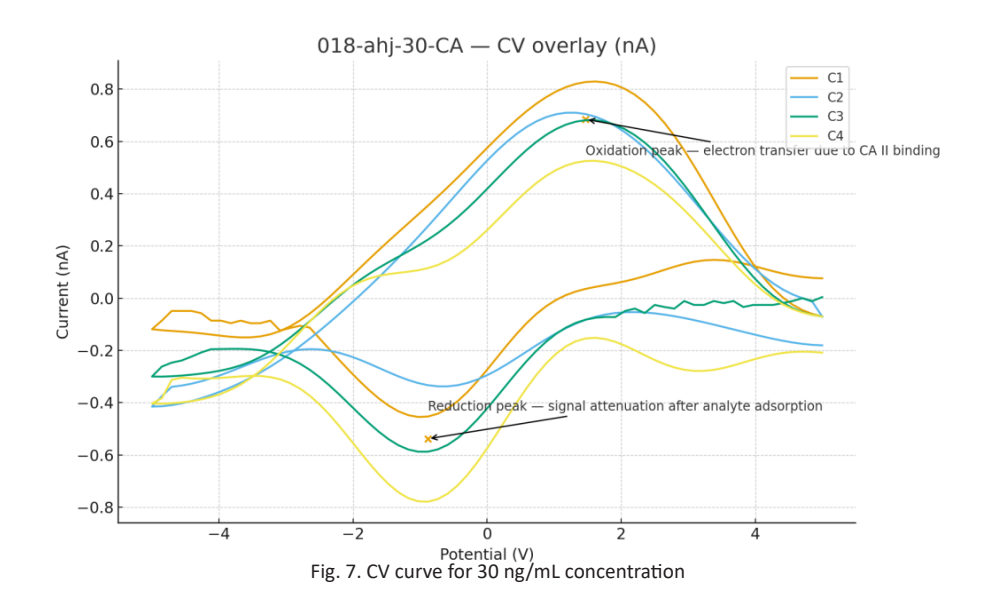
# 10 ng/mL

At this low concentration, CA II molecules begin to bind to the active sites on the electrode surface. Consequently, the oxidation peak current decreases to  $\approx 0.59$  nA, and the total charge decreases to  $\approx -15.7$  nC. This reduction indicates

the formation of a thin protein layer that partially blocks electron transfer pathways, producing a clear and measurable response relative to the blank.

# 30 ng/mL

As the concentration increases, more CA II molecules bind to the surface, yet the oxidation peak current slightly increases to  $\approx 0.77$  nA while the charge continues to decrease to  $\approx -14.2$  nC. This dual behavior suggests protein reorganization on the electrode surface, where the adsorbed



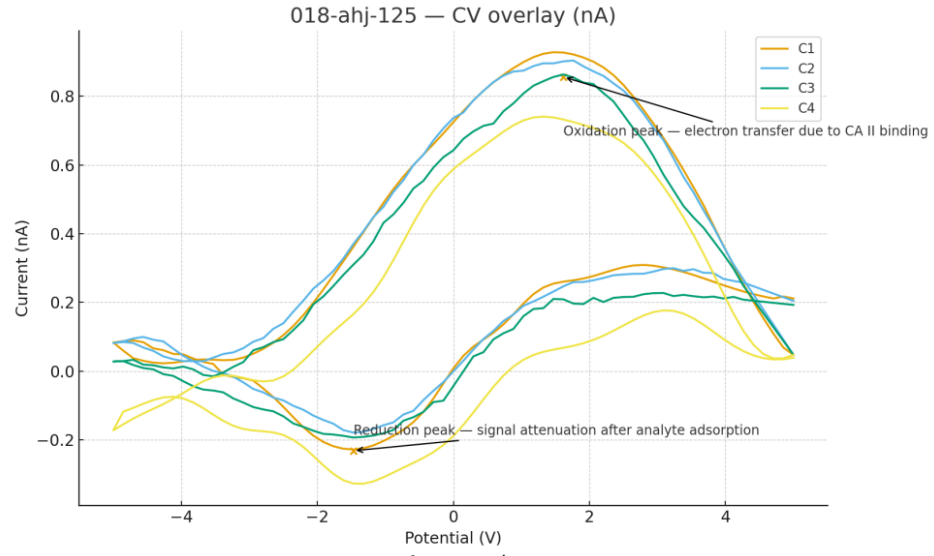


Fig. 8. CV curve for 125  $\,\mathrm{ng/mL}$  concentration

Table 1. Key Analytical Metrics

Parameter	Observed Value	Interpretation
Q trend (Charge Behavior)	Decreasing with concentration	Confirms signal-off behavior and analyte adsorption
RSD% (Reproducibility)	< 10%	Stable and repeatable response across four cycles
R <sup>2</sup> (Calibration Linearity)	≈ 0.97	Excellent linear correlation across 0–125 ng/mL
LOQ (Limit of Quantification)	≈ 15–20 ng/mL	Accurate quantification region starts above 10 ng/mL
LOD (Limit of Detection)	≈ 5–7 ng/mL	Sensitive enough to detect below the lowest tested concentration (10 ng/mL)

layer becomes more compact while still leaving limited electron transport channels available. This stage is commonly observed in biosensors near pre-saturation binding levels.

### 125 ng/mL

At high CA II concentration, dense protein accumulation occurs on the electrode surface. This leads to a reorganization effect that creates localized electron transfer pathways, which is reflected by an increase in the oxidation peak current to  $\approx 0.83$  nA and a rise in charge to  $\approx -24.4$  nC. This behavior is known as the surface reorganization effect, confirming that the sensor response is concentration-dependent and arises from specific interaction with the target protein.

# Electrochemical Sensor Evaluation for CA II Detection

Based on the cyclic voltammetry (CV) analysis and extracted charge (Q) values, current (Ip) from four consecutive cycles at, CA II concentrations ranging from 0 to 125 ng/mL, the AuNP/CNT/PAni/PVA composite electrode deposited on a gold substrate exhibited a clear dose—response behavior. Both the total charge (Q) and the oxidation current decreased progressively with increasing CA II concentration, indicating effective electron-transfer modulation due to specific antigen binding at the electrode surface (Table 1).

### CONCLUSION

The AuNP/CNF/PAni/PVA-based electrochemical sensor demonstrates reliable sensitivity and selectivity toward the CA II biomarker. The clear dose-dependent signal suppression, high linearity (R²  $\approx$  0.97), and low LOD (~5–7 ng/mL) indicate that the sensor effectively detects CA II within the studied range (0–125 ng/mL). The low RSD (<10%) further supports film stability and consistent electrochemical response. Hence, this sensor can be considered a promising platform for cancer biomarker detection using CV techniques.

### **CONFLICT OF INTEREST**

The authors declare that there is no conflict of interests regarding the publication of this manuscript.

#### **REFERENCES**

- Haleem A, Javaid M, Singh RP, Suman R, Rab S. Biosensors applications in medical field: A brief review. Sensors International. 2021;2:100100.
- Hang Y, Wang A, Wu N. Plasmonic silver and gold nanoparticles: shape- and structure-modulated plasmonic functionality for point-of-caring sensing, bioimaging and medical therapy. Chemical Society Reviews. 2024;53(6):2932-2971.
- Arham Z, Nurdin M, Kurniawan K, Ismaun I, Maulidiyah M, Umar AA, et al. Promising Multi-Oxide Decorated Graphene Nanomaterials from Nickel Slag for Voltammetric Sensor Electrodes. Water, Air, and Soil Pollution. 2025;236(7).
- Gergeroglu H, Yildirim S, Ebeoglugil MF. Nano-carbons in biosensor applications: an overview of carbon nanotubes (CNTs) and fullerenes (C60). SN Applied Sciences. 2020;2(4).
- Zhang Z, Wan M. Composite films of nanostructured polyaniline with poly(vinyl alcohol). Synthetic Metals. 2002;128(1):83-89.
- Zhang H, Jiang S, Duan G, Li J, Liu K, Zhou C, et al. Heat-resistant polybenzoxazole nanofibers made by electrospinning. Eur Polym J. 2014;50:61-68.
- Devi LS, Paily R, Dasmahapatra AK. Platinum embedded conducting polyaniline/polyvinyl alcohol hydrogel for enhanced glucose biomolecule detection. Polymer. 2025;317:127947.
- Adabi M, Esnaashari SS, Adabi M. An electrochemical immunosensor based on electrospun carbon nanofiber mat decorated with gold nanoparticles and carbon nanotubes for the detection of breast cancer. Journal of Porous Materials. 2020;28(2):415-421.
- 9. Kumar S, Tripathy S, Singh OK, Singh SG. Cerium oxide nanofiber based electroanalytical sensor for TNF- $\alpha$  detection: Improved interfacial stability with Nafion. Bioelectrochemistry. 2021;138:107725.
- Oluwatosin Abegunde O, Titilayo Akinlabi E, Philip Oladijo O, Akinlabi S, Uchenna Ude A. Overview of thin film deposition techniques. AIMS Materials Science. 2019;6(2):174-199.
- Hwang HS, Jeong JW, Kim YA, Chang M. Carbon Nanomaterials as Versatile Platforms for Biosensing Applications. Micromachines. 2020;11(9):814.
- Paimard G, Shahlaei M, Moradipour P, Karamali V, Arkan E. Impedimetric aptamer based determination of the tumor marker MUC1 by using electrospun core-shell nanofibers. Microchimica Acta. 2019;187(1).
- 13. Hong L, Qiu P, Niu S, Chen Q, Lu X, Chen F, et al. On-Site

(CO) BY

- Electrospinning Nanofiber Membranes Incorporating V-Shaped Organic Semiconductors for Multifunctional Diabetic Wound Dressing. Advanced Fiber Materials. 2024;6(5):1413-1427.
- Sempionatto JR, Moon J-M, Wang J. Touch-Based Fingertip Blood-Free Reliable Glucose Monitoring: Personalized Data Processing for Predicting Blood Glucose Concentrations. ACS Sensors. 2021;6(5):1875-1883.
- 15. Lakhera P, Chaudhary V, Kush P, Kumar P. Nanomaterial-mediated biosensors. Multifunctional Nanocarriers: Elsevier; 2022. p. 523-553.
- Juska VB, Pemble ME. A Critical Review of Electrochemical Glucose Sensing: Evolution of Biosensor Platforms Based on Advanced Nanosystems. Sensors. 2020;20(21):6013.
- 17. Naresh V, Lee N. A Review on Biosensors and Recent Development of Nanostructured Materials-Enabled Biosensors. Sensors. 2021;21(4):1109.
- Alousi MAA, Naeem GA, Alghafour NMA, Mohammad SM. Characteristics of TiO<sub>2</sub>-Cu thin films deposited using electrospray technique. International Journal of Nanotechnology. 2022;19(2/3/4/5):186.
- Alalousi MM, Rzaij JM, Ibrahim IM, Ramizy A, Eisa MH. Sensing Enhancement of Gold Nanoparticles Doped-TiO,

- Thin Films as  $\rm H_2S$  Gas Sensor. Nano Hybrids and Composites. 2022;35:1-10.
- Epp J. X-ray diffraction (XRD) techniques for materials characterization. Materials Characterization Using Nondestructive Evaluation (NDE) Methods: Elsevier; 2016. p. 81-124.
- Babu Killana K, Devi Killana R. I -V Simulation of Amperometric Biosensor in Detection of Cancer through Cyclic Voltammetry Technique. 2022 International Conference on Breakthrough in Heuristics And Reciprocation of Advanced Technologies (BHARAT); 2022/04: IEEE; 2022. p. 1-4.
- Ebrahimi Vafaye S, Rahman A, Safaeian S, Adabi M. An electrochemical aptasensor based on electrospun carbon nanofiber mat and gold nanoparticles for the sensitive detection of Penicillin in milk. Journal of Food Measurement and Characterization. 2020;15(1):876-882.
- 23. Wang J, Yue X, Zhang Y, Zhu C, Kang X, Yu H-D, et al. Plasmonic Sensing of Glucose Based on Gold–Silver Core—Shell Nanoparticles. Chemosensors. 2022;10(10):404.
- Liu Z, Wang H, Li J, Wang M, Yang H, Si F, et al. Detection of exosomes via an electrochemical biosensor based on C60-Au-Tb composite. Microchem J. 2021;170:106772.

J Nanostruct 16(1): 279-287, Winter 2026